NUMERICALLY EFFICIENT LOW-THRUST COLLISION AVOIDANCE MANEUVER DESIGN IN GEO REGIME WITH EQUINOCTIAL ORBITAL ELEMENTS

A. De Vittori[(1)], G. Dani[(2)], P. Di Lizia[(3)], and R. Armellin[(4)]

[(1)]*Department of Aerospace Engineering, Politecnico di Milano, Via Privata Giuseppe La Masa 34, Milano, Lombardia, Italia 20156. Email: andrea.devittori@polimi.it*

[(2)]*Department of Aerospace Engineering, Politecnico di Milano, Via Privata Giuseppe La Masa 34, Milano, Lombardia, Italia 20156. Email: gabriele.dani@mail.polimi.it*

[(3)]*Department of Aerospace Engineering, Politecnico di Milano, Via Privata Giuseppe La Masa 34, Milano, Lombardia, Italia 20156. Email: pierluigi.dilizia@polimi.it*

[(4)]*Department of Aerospace Engineering, University of Auckland, 20 Symonds Street, Auckland Central, Auckland, New Zealand 1010. Email: roberto.armellin@auckland.ac.nz*

ABSTRACT

This work presents novel approaches to combined Collision Avoidance Maneuver (CAM) and station-keeping design in the geostationary regime in the case of low-thrust propulsion systems. By assuming short-term encounters, the resulting optimal control problem results in a fully analytical solution with a Multi-Point Boundary Value Problem (MPBVP) formulation. Having tight constraints in the satellite slot allocation makes the station-keeping target state pivotal to maximize the resident time within the box. Two strategies are applied to find the candidate state and compared in terms of maneuver planning. Ultimately, the needed computational time for CAM planning ensures the feasibility of future onboard implementation.

Keywords: Space Debris, Collision Avoidance, Station-keeping, Low-thrust, SST.

1. INTRODUCTION

Space debris mitigation is a hot topic in the science community because possible cascading effects may threaten the future of space missions. Since the beginning of the space era, thousands of satellites have been launched, and among active and inactive satellites, over 23,000 objects are regularly tracked in the Near Earth environment. Tinier fragments, hard to detect with modern-day technologies, compose the majority of all high-speed clutter and spread across all domains of interest. The Low Earth orbital (LEO) and Geosynchronous Earth Orbit (GEO) are the most populated realms. The latter plays a crucial role in communication, observation, and weather forecast. Objects living in GEO are mainly upper stages, apogee boost motors, and mission-related tools like deployment hardware and instrument covers. The above list enlarges with non-operational satellites representing a potential hazard to other active satellites once they reach the end of life [ESA22]. In this regime, the satellite's natural motion, affected by the geopotential perturbation, induces the satellite to get away from the assigned station-keeping box bounded by sharp latitude and longitude values. Frequent Station-Keeping (SK) cycles push the spacecraft to remain inside the indicated slot to prevent interferences with neighbouring satellites. That said, close calls with a piece of space debris are becoming more likely to happen during these routines. For this reason, ground controllers anticipate or delay SK maneuvers sacrificing fuel consumption. Hence, designing effective Collision Avoidance Maneuvers (CAMs) is becoming vital to preserving satellites in this regime. Moreover, given recent low-thrust propulsion technology findings, more satellites are moving toward this propulsion system. Albeit the state-of-the-art low-thrust CAM is booming, no one presents a procedure to combine CAMs and SK as an all-in-one solution. Research on low-thrust optimization methods encompasses the semi-analytical policy devised by Reiter et al. [RS18] for rapid collision avoidance, featuring an optimal radial thrust valid for just-in-time maneuvers. In 2022, De Vittori [Pal21] implemented an analytic formulation for the energy-optimal CAM enforcing a Probability of Collision (PoC) Threshold at TCA as a terminal constraint leveraging cartesian and Bplane coordinates. The policy serves as a first-guess solution to Fuel-Optimal (FO) CAM shaped by a bang-bang acceleration to the detriment of a time-consuming algorithm. More semi-analytical methods were proposed in [GGCDL19]; this work exploits average dynamics maximizing the miss distance by assuming continuous tangential thrust. Bombardelli and Hernando-Ayuso [HAB21a] focused instead on the problem of optimum low-thrust collision avoidance between two objects applicable to just circular orbits with constant thrust magnitude. The optimal control is framed in B-plane coordinates to curb the number of state variables. Martinez Chamarro et al. [MCBHA21] proposes a bang-bang solution scheme by

applying a smoothing approach to energy optimal continuous solution and one based on convex optimization. In 2012, Lee conceived a collision avoidance maneuver for LEO and Geostationary Earth Orbit (GEO) satellites maintained in a keeping area [LKS12].
This work takes inspiration from [Can22], and the goal is to find a computationally efficient CAM to meet a target Probability of Collision (PoC) and maximize the permanence time within the box. An Energy Optimal Control Problem (EOCP) CAM is devised as the analytical solution to a three-point boundary value problem (3PBVP). Tailored conditions are the initial maneuvering point, the minimum PoC threshold at TCA, and a target terminal state. Dynamics-wise, the Equinoctial Orbital Elements (EOEs) ensure computational efficiency if compared to the standard ECI formulation. The analytical solution retrieves by leveraging a first-order motion approximation to turn the Energy-Optimal (EO) CAM into an Initial Value Problem. The linearization is performed via two State Transition Matrices linking state and costate variations from the initial point to TCA and from TCA to the final time. The problem-solution can distinguish between two possible scenarios. On one side, station-keeping alone is enough to ensure a PoC lower than a safeguard limit. On the other hand, when not fulfilling this requirement, the algorithm autonomously detects the best strategy for commanding CAM and station-keeping by imposing an arbitrary PoC at TCA without engineering a new CAM.

2. FUNDAMENTALS

This section defines the theoretical knowledge needed for the analytical CAM formulation.

2.1. Conjunction definition

In this work, CAMs are planned within the short-term encounter hypothesis between a satellite and debris. The maneuverable object (primary) identifies with $\mathbf{x}_p = [\mathbf{r}_p; \mathbf{v}_p]$ while debris (secondary) by $\mathbf{x}_s = [\mathbf{r}_s; \mathbf{v}_s]$. $\mathbf{r}_i$ and $\mathbf{v}_i$ link to the objects' center of mass set in a generic frame $\hat{\Re}$. In this context, the Bplane has been extensively adopted in the literature to capture collision geometry and probability. The origin of this frame is at the centre of the secondary object at conjunction as seen in Fig. 1, with the following axes direction:

$$\mathbf{u}_\xi = \frac{\mathbf{v}_p \times \mathbf{v}_s}{||\mathbf{v}_p \times \mathbf{v}_s||},\ \mathbf{u}_\eta = \frac{\mathbf{v}_p - \mathbf{v}_s}{||\mathbf{v}_p - \mathbf{v}_s||},\ \mathbf{u}_\zeta = \mathbf{u}_\xi \times \mathbf{u}_\eta \tag{1}$$

The position vector in BPlane coordinates is associated with $\mathbf{b}_{3D} = [\xi, \eta, \zeta]^\top$. The rotation matrix to pass from the inertial reference to the B-Plane one is defined as:

$$\mathbf{R}_{b,3D} = [\mathbf{u}_\xi, \mathbf{u}_\eta, \mathbf{u}_\zeta]^\top \tag{2}$$

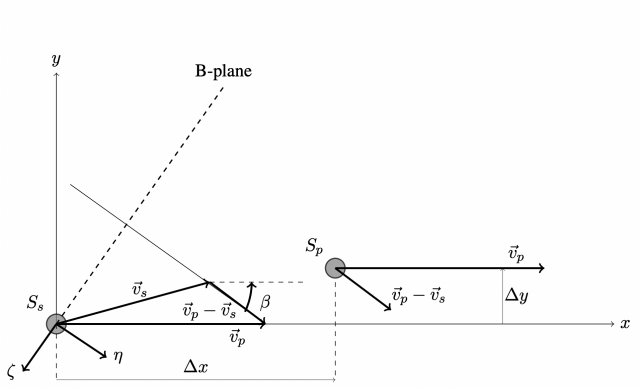

Figure 1: BPlane representation [Bom13]

Thus, the projection on the η axis becomes:

$$\mathbf{R}_{b,2D} = [\mathbf{u}_\xi, \mathbf{u}_\zeta]^\top \tag{3}$$

and the 2D BPlane position vector is $\mathbf{b} = [\xi, \zeta]^\top$.

2.2. Chan's PoC model

PoC between two likely colliding objects in a short-term encounter stems from the integration of the relative position probability density function over a sphere of radius R_A at TCA (i.e. the hard body sphere obtained by summing the primary and secondary radii). This assumption holds just with tridimensional shapes where all dimensions are comparable in size. No information about the attitude is needed whether dealing with a sphere [HAB21b]. If the relative probability distribution function is Gaussian, the approximated Chan's method of equivalent cross-sectional areas computes the collision probability with a convergent series:

$$\mathrm{PoC}(u, v) = e^{-\frac{v}{2}} \sum_{m=0}^{\infty} \frac{v^m}{2^m m!} \left[1 - e^{-\frac{u}{2}} \sum_{k=0}^{m} \frac{u^k}{2^k k!} \right] \tag{4}$$

Where u is the ratio of the impact cross-sectional area to the 1σ B-Plane covariance ellipse area:

$$u = \frac{s_A^2}{\sigma_\xi \sigma_\zeta \sqrt{1 - \rho_{\xi\zeta}^2}} \tag{5}$$

and v is the Squared Mahalanobis Distance (SMD):

$$\begin{aligned} v &= (\mathbf{r}_p - \mathbf{r}_s)^\top \mathbf{R}_{b,2D}^\top \mathbf{C}^{-1} \mathbf{R}_{b,2D} (\mathbf{r}_p - \mathbf{r}_s) = \\ &= \mathbf{b}_p^\top \mathbf{C}^{-1} \mathbf{b}_p \end{aligned} \tag{6}$$

where: $\mathbf{C}$ is the covariance matrix, and $\mathbf{b}_p$ is the primary object position relative to the secondary in the BPlane coordinates.

2.3. Dynamics of Geostationary satellites

The EOE entails the motion linearization around the station-keeping nominal condition. A thorough analysis of this set of elements is disclosed by Gazzino in [Gaz17] and [GAL+16] :

$$\mathbf{x_{eoe}} = \begin{bmatrix} a \\ e_x = e\cos\omega + \Omega \\ e_y = e\sin\omega + \Omega \\ i_x = \tan\frac{i}{2}\cos\Omega \\ i_y = \tan\frac{i}{2}\sin\Omega \\ l_{M\Theta} = \Omega + \omega + M - \Theta \end{bmatrix} \qquad \mathbf{a_c} = \begin{bmatrix} a_n \\ a_t \\ a_h \end{bmatrix} \tag{7}$$

Where Θ represents Greenwich right ascension.

The correspondent non-linear dynamics is expressed as:

$$\frac{d\mathbf{x_{eoe}}}{dt} = \mathbf{f_l}(\mathbf{x_{eoe}}, t) + \mathbf{f_g}(\mathbf{x_{eoe}}, t)\mathbf{a_c} \tag{8}$$

$\mathbf{f_l}$ is the Lagrange contribution part of the external force model described by the CNES ORANGE model [CB94] and $\mathbf{f_g}$ is the Gauss contribution part. Introducing the nominal keeping position:

$$\begin{aligned} &\mathbf{x_{sk}} = [a_{sk}, 0, 0, 0, 0, l_{M\Theta,sk}]^T \\ &\frac{d\mathbf{x_{sk}}}{dt} = \left[0, 0, 0, 0, 0, \sqrt{\tfrac{\mu}{a_{sk}^3}} - \omega_T\right]^T = \mathbf{0} \end{aligned} \tag{9}$$

It is now possible to define a dynamical model based on the relative state:

$$\begin{aligned} &\mathbf{x} = \mathbf{x_{eoe}} - \mathbf{x_{sk}} \\ &\frac{d\mathbf{x}}{dt} = \mathbf{f_l}(\mathbf{x_{eoe}}, t) + \mathbf{f_g}(\mathbf{x_{eoe}}, t)\mathbf{u} - \mathbf{0} \end{aligned} \tag{10}$$

It linearizes through a first-order linearization:

$$\begin{aligned} &\mathbf{A}(t) = \left.\frac{\partial \mathbf{f_l}}{\partial \mathbf{x}}\right|_{\mathbf{x_{sk}}} \qquad \mathbf{D}(t) = \mathbf{f_l}(\mathbf{x_{sk}}, t) \\ &\mathbf{B}(t) = \mathbf{f_g}(\mathbf{x_{sk}}, t) \end{aligned} \tag{11}$$

The control matrix $\mathbf{B}$ can be found in [LLD+06]. The equations of motion are then:

$$\dot{\mathbf{x}} = \mathbf{A}(t)\mathbf{x} + \mathbf{D}(t) + \mathbf{B}(t)\mathbf{u} \tag{12}$$

2.4. Geopotential perturbations in GEO

The Geopotential perturbation leads satellites to depart during their motion from the mission-defined trajectory. In its mathematical formulation the Earth gravity potential, labelled with W, depends on the geocentric radial distance (r), the geocentric latitude (ψ), and the geocentric longitude (λ) [Dea98]. In particular:

$$W(r, \psi, \lambda) = V_W(r, \psi, \lambda) + R(r, \psi) \tag{13}$$

where V_W is the gravitational potential and R is the rotational potential of the Earth that has the following shapes:

$$\begin{aligned} V_W(r, \psi, \lambda) = &\frac{GM}{r}\left[1 + \sum_{n=2}^{N}\left(\frac{a}{r}\right)^n \sum_{m=0}^{n}\right. \\ &\left.(C_n^m cos(m\lambda) + S_n^m sin(m\lambda))P_n^m(t)\right] \end{aligned} \tag{14}$$

$$W(r, \psi) = \frac{\omega^2}{2}(rcos\psi)^2 \tag{15}$$

r, ψ, λ are polar coordinates, $t = sin\psi$, GM is the product between the Earth's gravitational constants and the Earth's mass, a is the semi-major axis of the reference orbit, n and m are positive integers or zero, C_n^m and S_n^m are geopotential coefficients of n^{th} degree and m^{th} order, $P_n^m(t)$ are the associated Legendre functions, and N is the maximum degree and order of the available coefficients. Just the contributions up to $J_{2,2}$ ($N = 2$) are considered because responsible for the longitude drift. Its effect on the dynamics translates to a modification of the state matrix $\mathbf{A}$ and the vector $\mathbf{D}$ with a dual decomposition:

$$\begin{aligned} \mathbf{A}(t) &= \mathbf{A_{kep}}(t) + \mathbf{A_{J2}}(t) \\ \mathbf{D}(t) &= \mathbf{D_{kep}}(t) + \mathbf{D_{J2}}(t) \end{aligned} \tag{16}$$

For more information about their derivation refer to [Gaz17].

2.5. State Transition Matrix

The STM, evaluated on a reference dynamics and labelled with $\mathbf{\Phi}$, maps any sufficiently small state variation at a certain time t_0 to a final one at t_f:

$$\delta\mathbf{x}_f = \mathbf{\Phi}\delta\mathbf{x}_0 \tag{17}$$

For time-varying systems, $\mathbf{\Phi}(t, t_0)$ is the solution of this set of differential equations:

$$\dot{\mathbf{\Phi}}(t, t_0) = \mathbf{A}(t)\mathbf{\Phi}(t, t_0),\ \mathbf{\Phi}(t_0, t_0) = \mathbf{I} \tag{18}$$

where $\mathbf{\Phi}(t_0, t_0)$ is the initial condition and $\mathbf{A}(t)$ is jacobian matrix associated with $\boldsymbol{f}(\mathbf{x}, t)$ around the nominal trajectory $\mathbf{x}_n$:

$$\mathbf{A} = \left.\frac{\partial \boldsymbol{f}(\mathbf{x}, t)}{\partial \mathbf{x}}\right|_{\mathbf{x}_n} \tag{19}$$

3. LOW-THRUST ENERGY-OPTIMAL CAM AND SK DESIGN IN GEO ORBIT

Due to strict slot allocation, spacecraft in the GEO ring are confined within a box with sharp longitude and latitude boundaries. The deviation from the reference trajectory is governed by the orbital perturbations. In particular, the non-spherical Earth perturbation mainly affects

the longitude evolution, while the Solar and Moon perturbations modify the latitude one. Here, the problem formulation limits to considering the Earth's geopotential in the analytical CAM design with embedded station-keeping.

3.1. Analytical optimal control problem derivation

The dynamical model is built upon the EOE coordinates set. The Energy-Optimal (EO) problem starts from the statement of a cost function minimizing the energy:

$$J := \nu\xi(t_{ca}, \mathbf{x}(t_{ca})) + \int_{t_i}^{t_f} \frac{1}{2}{\mathbf{a_c}}^T \mathbf{a_c} dt \tag{20a}$$

$$\xi(t_{ca}, \mathbf{x}(t_{ca})) = SMD(\mathbf{r}(t_{ca})) - \overline{SMD} \geq 0 \tag{20b}$$

By introducing the concept of the hamiltonian function as:

$$H := \frac{1}{2}{\mathbf{a_c}}^T \mathbf{a_c} + \boldsymbol{\lambda}^T \mathbf{f}(\mathbf{x}, \mathbf{a_c}) \tag{21}$$

And by imposing the first variation of the functional to zero, the corresponding Euler-Lagrange Equations are:

$$\begin{cases} \left.\dfrac{\partial \mathbf{x}}{\partial \eta}\right|_{t_i} = 0 \\ \left.\dfrac{\partial \mathbf{x}}{\partial \eta}\right|_{t_f} = 0 \\ \dfrac{\partial H}{\partial \mathbf{a_c}} = {\mathbf{a_c}}^T + \boldsymbol{\lambda}^T \mathbf{B}(t) = \mathbf{0} \Longrightarrow \mathbf{a_c} = -\mathbf{B}(t)^T \lambda \\ \dfrac{\partial H}{\partial \mathbf{x}} + \dot{\boldsymbol{\lambda}}^T = 0 \Longrightarrow \dot{\boldsymbol{\lambda}} = -\mathbf{A}(t)^T \boldsymbol{\lambda} \\ \dfrac{\partial H}{\partial \boldsymbol{\lambda}} = \dot{\mathbf{x}} = \mathbf{f}(\mathbf{x}, \mathbf{a_c}) \\ \nu\xi(t_{ca}, \mathbf{x}(t_{ca})) = 0 \\ \nu \geq 0 \end{cases} \tag{22}$$

Solving for $\frac{\partial H}{\partial \mathbf{a_c}}$ leads to the MPBVP reported below:

$$\begin{cases} \dot{\mathbf{x}} = \mathbf{A}(t)\mathbf{x} - \mathbf{B}(t)\mathbf{B}(t)^T \boldsymbol{\lambda} + \mathbf{D}(t) \\ \dot{\boldsymbol{\lambda}} = -\mathbf{A}(\mathbf{t})^t \boldsymbol{\lambda} \end{cases} \tag{23a}$$

$$BCs: \begin{cases} \mathbf{x}(t_0) = \mathbf{x_0} \\ \mathbf{x}(t_f) = \mathbf{x_f} \\ \nu \dfrac{\partial \xi}{\partial \mathbf{x}(t_{ca})} - \boldsymbol{\lambda}^T(t_{ca}^-) + \boldsymbol{\lambda}^T(t_{ca}^+) = 0 \\ \nu\xi(t_{ca}, \mathbf{x}(t_{ca})) = 0 \\ \nu \geq 0 \end{cases} \tag{23b}$$

Worth noting that it can be either a 2PBVP or a 3PBVP in the light of the combination of initial and final state conditions and the SMD inequality. For instance, if station-keeping alone satisfies the inequality on SMD, ν will be null, and no costate discontinuity occurs at TCA. On the other hand, if the afore-mentioned condition is not met, ν will be different from zero to impose the equality constraint on SMD. The latter will require stopping and restarting the integration at conjunction with the updated costates.

3.2. Target Definition

The targeted set of EOE elements at t_f should guarantee the maximum resident time within the station-keeping box after CAM. This dissertation presents two possible alternatives.

3.2.1. Analytical definition

The first approach determines the ideal target longitude under the geopotential perturbation. It does not output the full state, but only the optimal semi-major axis and the longitude; the others are set to zero. The problem-solution takes inspiration from [Soo94]. The longitudinal acceleration due to J_{22} is tabulated for different values of longitude.

$$\ddot{l}_m(t) = A = const \tag{24a}$$

$$\dot{l}_m(t) = At + \dot{l}_m(0) \tag{24b}$$

$$l_m(t) = \frac{1}{2}At^2 + \dot{l}_m(0)t + l_m(0) \tag{24c}$$

Acting on the semi-major axis tweaks the longitude drift rate. The complete mathematical formulation can be found in [Soo94]:

$$\dot{l}_m = -\frac{3}{2}\frac{\omega_E}{a_{GEO}}\Delta a \tag{25}$$

Where ω_E is the Earth's rotational angular velocity, a_{GEO} is the semi-major axis of geostationary orbit a and Δa its offset. These two pieces of information are sufficient to solve the problem. The procedure is then:

1. For the assigned $\overline{l_m}$ compute the tabulated value of longitudinal acceleration. initial longitude as:

$$\begin{cases} l_m(0) = \overline{l_m} + \dfrac{\delta}{2} \; if \; A > 0 \\ l_m(0) = \overline{l_m} - \dfrac{\delta}{2} \; if \; A < 0 \end{cases} \tag{26}$$

   Where δ is the admissible longitude window.

2. Use 24c to find $\dot{l}_m(0)$ and T by setting:

$$\begin{aligned} At \quad & t = T \quad & \Delta l_m(T) = \Delta l_m(0) \\ At \quad & t = \frac{T}{2} \quad & \Delta l_m\left(\frac{T}{2}\right) = -\Delta l_m(0) \end{aligned} \tag{27}$$

Leading to:

$$\begin{cases} \Delta l_m(0) = \frac{1}{2}AT^2 + \dot{l_m}(0)T + \Delta l_m(0) \\ -\Delta l_m(0) = \frac{1}{8}AT^2 + \dot{l_m}(0)\frac{T}{2} + \Delta l_m(0) \end{cases} \tag{28}$$

$$T = 4\sqrt{\frac{\Delta l_m(0)}{A}} = 4\sqrt{\frac{\delta}{2A}} \tag{29a}$$

$$\dot{l_m}(0) = -2sign(A)\sqrt{2A\delta} \tag{29b}$$

3. Get Δa from $\dot{l}_m(0)$ with the Eq. 25:

$$\Delta a = -\frac{3}{2}\frac{a_{GEO}}{\omega_E}\dot{l}_m(0) \tag{30}$$

3.2.2. Numerical definition

The second method consists in a numerical maximization of the resident time. The algorithm forwardly propagates the dynamics up to one of the bounds. Its reliability comes down to how accurately the model can depict the spacecraft's motion. The drawback resides in the computational burden that goes hand-in-hand with the model complexity and the number of integrations.

3.3. Analytical optimal control solution

Motion linearization with STMs about the uncontrolled trajectory serves to get an analytical CAM formulation:

$$\begin{cases} \dot{\mathbf{\Phi}}(t) = \mathbf{A_{STM}}(t)\mathbf{\Phi}(\mathbf{x}(t_0), t) \\ \mathbf{\Phi}(\mathbf{x}(t_0), t_0) = \mathbf{I} \end{cases} \tag{31}$$

Where:

$$\mathbf{A_{STM}}(t) = \begin{bmatrix} \mathbf{A}(t) & -\mathbf{B}(t)\mathbf{B}(t)^T \\ \mathbf{0_{3\times 3}} & -\mathbf{A(t)^T} \end{bmatrix} \tag{32}$$

For starters, evaluate the STM on the first branch $[t_0,\ t_{ca}^-]$.

$$\begin{bmatrix} \boldsymbol{\delta}\mathbf{x_{ca}} \\ \boldsymbol{\lambda}_{\boldsymbol{ca}-} \end{bmatrix} = \begin{bmatrix} \boldsymbol{\Phi}_{\boldsymbol{xx}} & \boldsymbol{\Phi}_{\boldsymbol{x\lambda}} \\ \boldsymbol{\Phi}_{\boldsymbol{\lambda x}} & \boldsymbol{\Phi}_{\boldsymbol{\lambda\lambda}} \end{bmatrix} \begin{bmatrix} \boldsymbol{\delta}\mathbf{x_0} \\ \boldsymbol{\lambda_0} \end{bmatrix} \tag{33}$$

Impose $\boldsymbol{\delta}\mathbf{x_0} = 0$, because the initial state is fixed at t_0 and compute $\boldsymbol{\lambda}_{\boldsymbol{ca}-}$ and $\boldsymbol{\delta x}_{\boldsymbol{ca}-}$:

$$\boldsymbol{\lambda}_{\boldsymbol{ca}-} = \boldsymbol{\Phi}_{\boldsymbol{\lambda\lambda}}\boldsymbol{\lambda_0} \tag{34a}$$

$$\boldsymbol{\delta}\mathbf{x}_{\mathbf{ca}^-} = \boldsymbol{\Phi}_{\boldsymbol{x\lambda}}\boldsymbol{\lambda_0} \tag{34b}$$

Substituting the second equation inside the first one:

$$\boldsymbol{\lambda}_{\boldsymbol{ca}-} = \boldsymbol{\Phi}_{\boldsymbol{\lambda\lambda}}\boldsymbol{\Phi}_{\boldsymbol{x\lambda}}{}^{-1}\boldsymbol{\delta}\mathbf{x_{ca}} = \mathbf{E}\boldsymbol{\delta}\mathbf{x_{ca}} \tag{35}$$

Recall the derivative of ξ:

$$\frac{\partial \xi}{\partial \mathbf{x}(t_{ca})} = \boldsymbol{\varphi}(\mathbf{x_{ca}}) \tag{36}$$

The co-state turns into:

$$\boldsymbol{\lambda}_{\boldsymbol{ca}+} = \boldsymbol{\lambda}_{\boldsymbol{ca}-} - \nu\boldsymbol{\varphi}(\mathbf{x_{ca}}) \tag{37}$$

To pass from EOE to the ECI reference frame, while preserving an analytical derivation, expand $\boldsymbol{\varphi}$ with zero order Taylor series expansion:

$$\boldsymbol{\varphi}(\mathbf{x_{ca}}) \approx \boldsymbol{\varphi}(\mathbf{x_{ref}}(t_{ca})) = \boldsymbol{\varphi} \tag{38}$$

As for the first arc, linearize the second one via STM:

$$\begin{bmatrix} \boldsymbol{\delta}\mathbf{x_f} \\ \boldsymbol{\lambda}_{\boldsymbol{f}} \end{bmatrix} = \begin{bmatrix} \boldsymbol{\Phi}_{\boldsymbol{xx}} & \boldsymbol{\Phi}_{\boldsymbol{x\lambda}} \\ \boldsymbol{\Phi}_{\boldsymbol{\lambda x}} & \boldsymbol{\Phi}_{\boldsymbol{\lambda\lambda}} \end{bmatrix} \begin{bmatrix} \boldsymbol{\delta}\mathbf{x_{ca}} \\ \boldsymbol{\lambda}_{\boldsymbol{ca}+} \end{bmatrix} \tag{39}$$

Take the first vectorial equation:

$$\boldsymbol{\delta}\mathbf{x_f} = \boldsymbol{\Phi}_{\boldsymbol{xx}}\boldsymbol{\delta}\mathbf{x_{ca}} + \boldsymbol{\Phi}_{\boldsymbol{x\lambda}}\boldsymbol{\lambda}_{\boldsymbol{ca}+} \tag{40}$$

Substitute EQ. 38, 35 and rearrange this expression:

$$\boldsymbol{\delta}\mathbf{x_f} = \mathbf{F}\boldsymbol{\delta}\mathbf{x_{ca}} - \nu\boldsymbol{\Phi}_{\boldsymbol{x\lambda}}\boldsymbol{\varphi} \tag{41}$$

Where:

$$\mathbf{F} = \boldsymbol{\Phi}_{\boldsymbol{xx}} + \boldsymbol{\Phi}_{\boldsymbol{x\lambda}}\mathbf{E}$$

$\boldsymbol{\delta}\mathbf{x_{ca}}$ is now function of ν from the previous relation:

$$\boldsymbol{\delta}\mathbf{x_{ca}} = \boldsymbol{\delta}\mathbf{x_{sk,ca}} + \nu\mathbf{h_{CAM}} \tag{42}$$

The two terms denote the contribution due to the station-keeping maneuver and CAM:

$$\boldsymbol{\delta}\mathbf{x_{sk,ca}} = \mathbf{F}^{-1}\boldsymbol{\delta}\mathbf{x_f} \qquad \mathbf{h_{CAM}} = \mathbf{F}^{-1}\boldsymbol{\Phi}_{\boldsymbol{x\lambda}}\boldsymbol{\varphi} \tag{43}$$

Remember that $\boldsymbol{\delta}\mathbf{x_f}$ is determined apriori being $\mathbf{x_f}$ the target state for station-keeping. At this stage, the algorithm splits in two. In the linearized dynamics, check if $\nu = 0$, $\xi(\mathbf{x_{sk,ca}}) \geq 0$ and retrieve $\boldsymbol{\lambda_0}$. $\mathbf{x_{sk,ca}} = \mathbf{x_{n,ca}} + \boldsymbol{\delta}\mathbf{x_{sk,ca}}$. $\mathbf{x_{sk,ca}}$ relates to the EOE elements of the primary at TCA on the nominal station-keeping trajectory, and $\mathbf{x_{n,ca}}$ is the EOE elements on the ballistic orbit at conjunction. If by chance this condition doesn't hold, the procedure will continue by enforcing $\xi(\mathbf{x_{ca}}) = 0$. Specify $\boldsymbol{\varrho}(\mathbf{x})$ as the function to convert the equinoctial orbital elements in ECI position coordinates.

$$\left[\boldsymbol{\varrho}(\mathbf{x_{ca}}) - \mathbf{r_s}(t_{ca})\right]^T \mathbf{Q}\left[\boldsymbol{\varrho}(\mathbf{x_{ca}}) - \mathbf{r_s}(t_{ca})\right] = \overline{SMD} \tag{44}$$

Where:

$$\mathbf{Q} = \mathbf{R_{2b}}^T\mathbf{C}^{-1}\mathbf{R_{2b}} \tag{45}$$

To ease the solution process, expand $\boldsymbol{\varrho}(\mathbf{x_{ca}})$ with a first-order Taylor expansion about $\mathbf{x_{sk,ca}}$:

$$\boldsymbol{\varrho}(\mathbf{x_{ca}}) \approx \mathbf{r_{sk,ca}}(t_{ca}) + \nu\mathbf{J}(\mathbf{x_{sk,ca}}(t_{ca}))\mathbf{h_{CAM}} \tag{46}$$

$\mathbf{r_{sk,ca}}$ defines the position of the primary at TCA with pure station-keeping. By abbreviating the notation:

$$\boldsymbol{\varrho}(\mathbf{x_{ca}}) \approx \mathbf{r_{sk,ca}}(t_{ca}) + \nu \mathbf{J}\mathbf{h_{CAM}} \tag{47}$$

Substitute the resulting expression inside Eq. 44:

$$\begin{aligned}&[\mathbf{r_{sk,ca}}(t_{ca}) + \nu \mathbf{J}\mathbf{h_{CAM}} - \mathbf{r_s}(t_{ca})]^T \mathbf{Q} \\ &\quad [\mathbf{r_{sk,ca}}(t_{ca}) + \nu \mathbf{J}\mathbf{h_{CAM}} - \mathbf{r_s}(t_{ca})] = \overline{SMD}\end{aligned} \tag{48}$$

Equation 48 solves in closed form as a second-order polynomial as a function of ν. Shortlist between the two roots, the one leading to a lower Δv in the linearized framework. To get $\boldsymbol{\lambda_0}$ follow the procedure backward. All the results shown in the next section are obtained with numerical integrations of the non-linear OCP.

3.4. Test Case

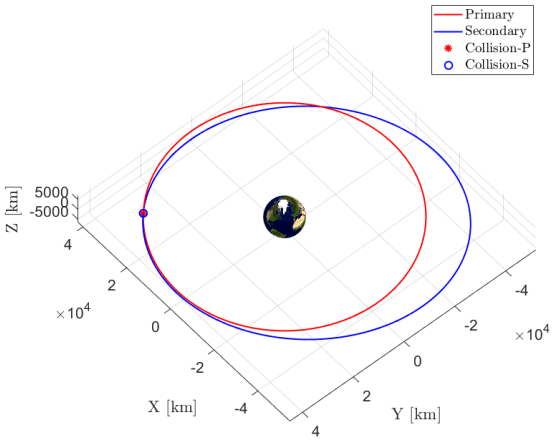

Figure 2: Test case GEO collision representation.

The proposed solution strategy applies to a test case kindly provided by the GMV company. An illustration of the resulting conjunction is pictured in Figure 2. Table 1 details the position and velocity vectors of the two involved objects at TCA in the ECI frame also covering PoC, SMD, and the miss distance d. The Keplerian elements of the two orbits are computed and displayed in Table 2.

Table 1: Test case conjunction data.

$\vec{r}_p$[km]	[2 8525, 3 1054, -42.4360]$^\top$
$\vec{r}_s$[km]	[2 8525, 3 1054, -42.4360]$^\top$
$\vec{v}_p$ [km/s]	[-2.2644, -2.0978, 0.0032]$^\top$
$\vec{v}_s$ [km/s]	[-2.3001, 2.2941, 0.4560]$^\top$
PoC	4.628e-02
SMD	0.2020
d [km]	0.0350

Table 2: Orbital elements, in order: semi-major axis, eccentricity, inclination, Right Ascension of the Ascending Node (RAAN), argument of the periapsis, true anomaly.

	a	e	i
O_p	42 165 km	4.4556e-05	0.8594 °
O_s	48 939 km	0.1441	8.00 °

	Ω	ω	θ
O_p	0 °	91.30 °	263.09 °
O_s	340.92 °	184.41 °	18.67 °

The osition covariance matrices of the two colliding RSO in the ECI reference frame are:

$$\vec{C}_p = \begin{bmatrix} 0.8085e-05 & -2.0477 & 6.55174 \\ -2.0477 & 137.6 & -1.8341e \\ 6.5517 & -1.8341 & 59.78 \end{bmatrix} \cdot 10^{-4} \text{ km}^2 \tag{49}$$

$$\vec{C}_s = \begin{bmatrix} 2.4481 & 7.2988 & 18.10 \\ 7.2988 & 0.1113 & -114.9 \\ 18.10 & -114.9 & 186.6 \end{bmatrix} \cdot 10^{-4} \text{ km}^2 \tag{50}$$

The corresponding combined covariance matrix in B-plane coordinates becomes:

$$\vec{C} = \begin{bmatrix} 687.7 & 564.7 \\ 0.0565 & 477.5 \end{bmatrix} \cdot 10^{-4} \text{ km}^2 \tag{51}$$

All the simulations showcased in this dissertation have run on an Intel(R) Core(TM) i7-10700 CPU processor with 16 GB of Ram Memory. Turning to the boundary conditions, the desired collision probability $PoC = 10^{-6}$ or equivalently $SMD = 17.1251$.

3.5. Analytical approach for final state target identification

The analytical target in Tab. 3 comes from the procedure sketched in Sect. 3.2.1. Figure 3 traces the logitude evolution over time revealing that the satellite stays bounded for nearly 40 days.

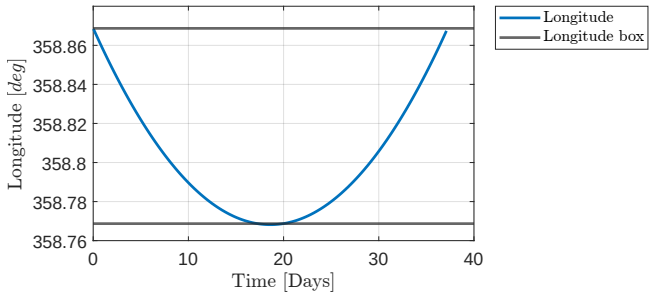

Figure 3: Target longitude evolution and longitude box.

Table 3: Analytical target.

a [km]	e_x	e_y	i_x	i_y	l_m [deg]
42 166.34	0	0	0	0	358.86

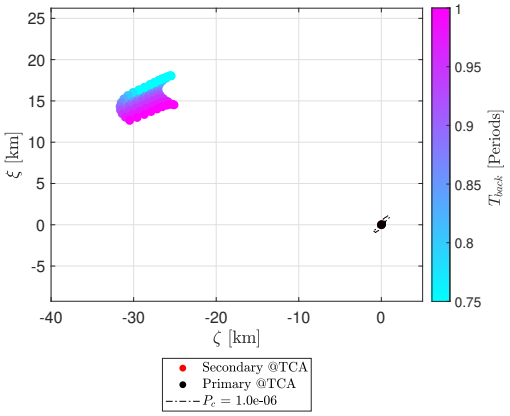

((a)) Bplane position for different T_{back}

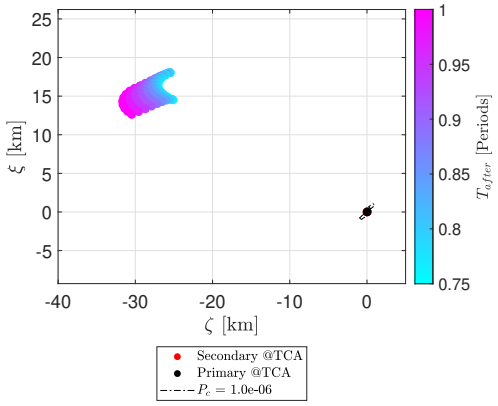

((b)) Bplane position for different T_{after}

Figure 4: Position of the primary object in the Bplane for the various values of t_{back} and t_{after}

To prove reliability, the primary is ensured not to fall within the iso-probability curve ($\xi \geq 0$) in Fig. 4(a) and 4(b). Each dot embeds the primary position in Bplane coordinates at TCA. The two graphs differ in the colour scheme, the former is sorted according to t_{back} i.e the time vector of initial maneuvering points, and t_{after} relates to the final integration time. In Fig. 5, given $\nu = 0$, no discontinuities affect the acceleration profile because only station-keeping applies.

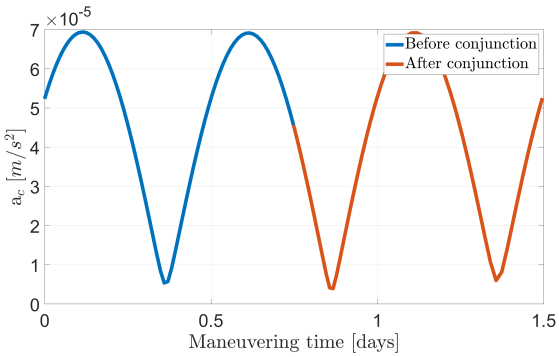

Figure 5: Acceleration magnitude profile of the primary object for $t_{back} = 0.75$ $[periods]$ and $t_{after} = 0.75$ $[periods]$.

Next, the output policy has to be compatible with a low-thrust propulsion system from Δv perspective as shown in Fig. 6.

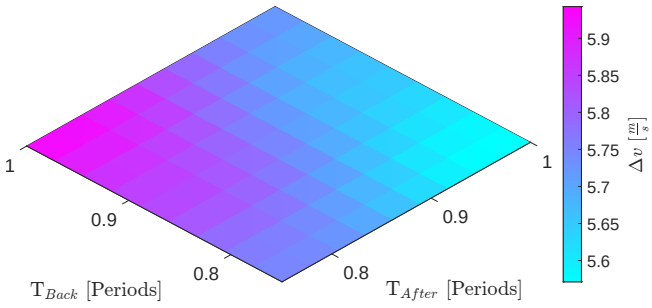

Figure 6: Δv for combined CAM and station-keeping

Among all possible t_{back} and t_{after} combinations, the one featuring the minimum Δv is further analyzed for some food for thought in Fig. 7(a) and 7(b). As far as longitude goes, it remains inside the station-keeping box during the entire maneuver. The same is not true for latitude; it appears to exceed the bounds to match the target at the final time. The OCP tends to rely on geopotential perturbation to lower the control effort. More tailored conditions may require the satellite to never cross the assigned slot at the expense of an analytical solution.

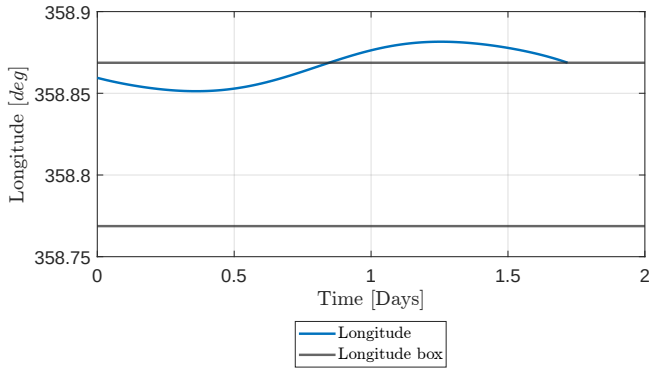

((a)) Longitude.

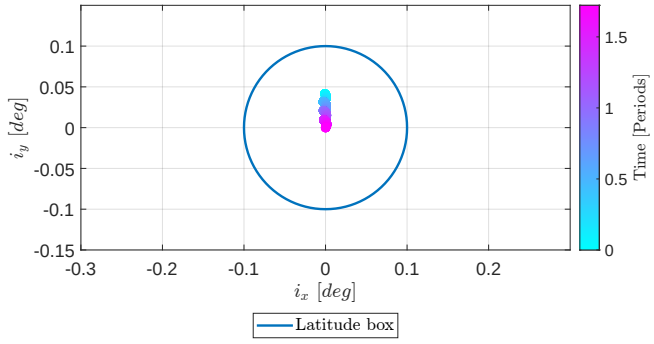

((b)) Latitude.

Figure 7: Spacecraft latitude and longitude evolution during the maneuver.

As clearly visible in Fig. 4(a) and 4(b), all the dots lie far away from the iso-probability curve $\nu = 0$). To assure that $\xi = 0$ works too, the station-keeping final condition is tweaked to make the CAM match $\overline{SMD}$ with an equality constraint. In addition, in Fig. 9, at TCA, enforcing a specific PoC level generates a discontinuity in the costates that reflects in the acceleration profile.

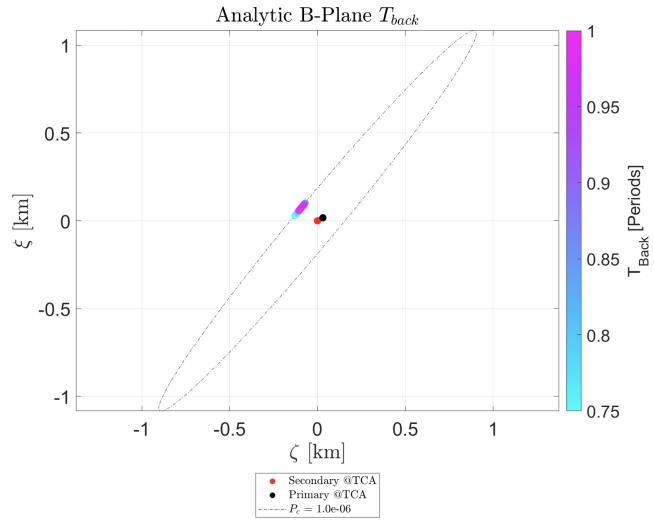

((a)) T_{back}.

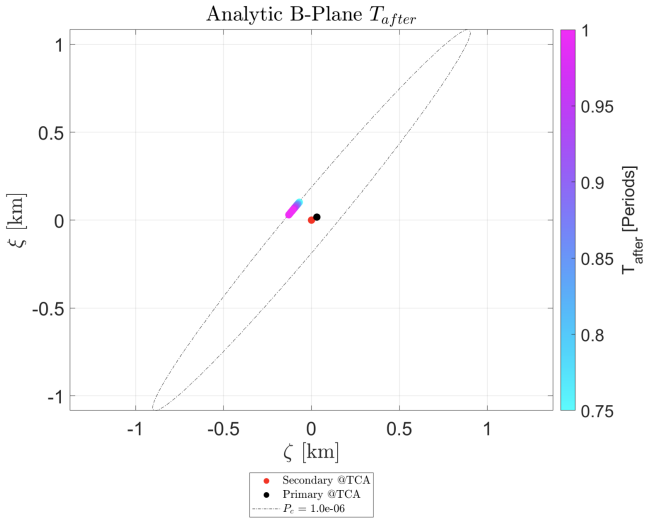

((b)) T_{after}.

Figure 8: B-plane position for $\xi = 0$.

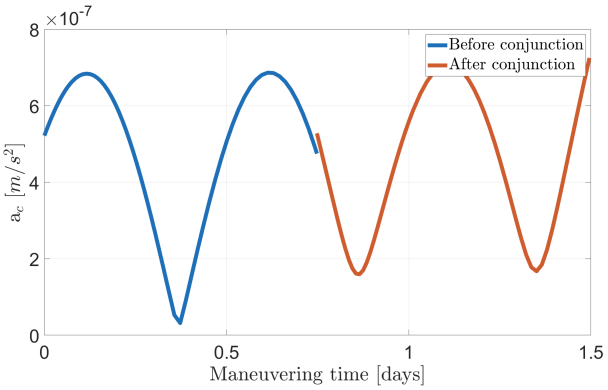

Figure 9: Acceleration magnitude profile of the primary object for $t_{back} = 0.75$ $[periods]$ and $t_{after} = 0.75$ $[periods]$

3.6. Numerical Target

Similarly to the analytical target, it is possible to represent in B-plane position for the various maneuvering points in Fig. 10(a) and 10(b). It seems that the analytical case in Fig. 4(b) and 4(a) and the numerical strategy make the primary end up in the same Bplane region. From a Δv standpoint, the maneuver cost almost mirrors the analytic one in Fig. 10.

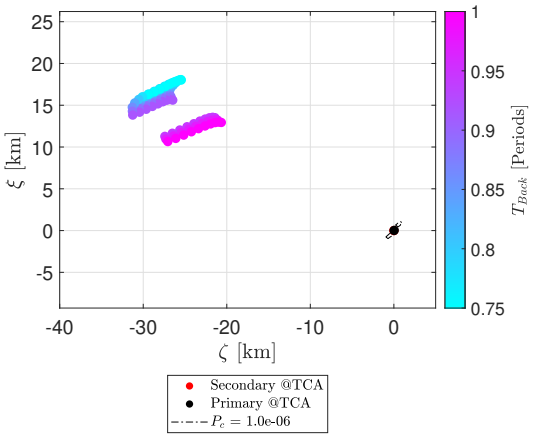

((a)) First trajectory arc.

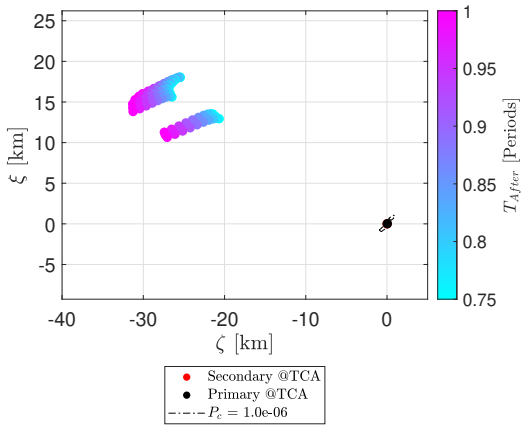

((b)) Second trajectory arc.

Figure 10: Position of the primary object in the Bplane for the various values of t_{back} and t_{after}

For what concerns the computational time, Fig. 12 reveals a strong dependency on the propagation time. The most demanding operation is the STM integration. The attained performance makes a future implementation of this routine promising for an onboard implementation or large-scale simulations.

4. CONCLUSIONS

This work makes a step forward to embedded CAM and station-keeping while retaining an analytical formulation.

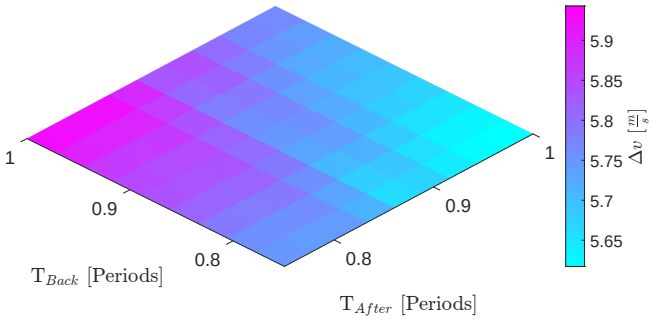

Figure 11: Δv maneuver cost

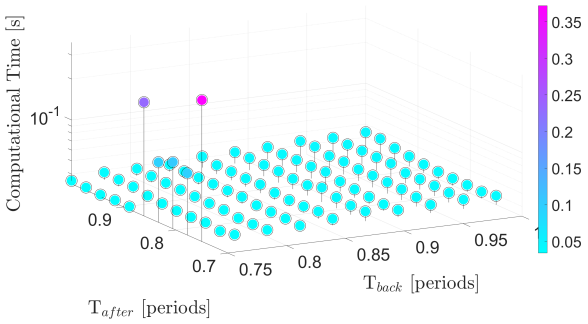

Figure 12: Computational time for the embedded CAM and Station-keeping

Starting from the work of A. Cantoni, an improved target final state estimation lets the spacecraft benefit from geopotential perturbation to maximize the resident time inside the SK box. CAM adopts the EOE elements as a new set of state variables to easily manage quantities of interest, such as latitude and longitude. The target elements are derived with an analytical and a numerical scheme with similar trends as Δv, and Bplane position go. Moving to computational time, the pipeline seems even brighter for future onboard execution. That said, there are still some open points and possible refinements. An effective and efficient bang-bang transformation would translate into an operative framework with additional fuel savings. It is also pivotal to include path constraints to prevent the spacecraft from exceeding the allocated slot while maneuvering. Moreover, other perturbation-like contributions may be encompassed: Solar Radiation Pressure and the third body perturbations. Ultimately, the geostationary ring is more affected than others by likely long-term encounters, but Chan's PoC fails at picturing the collision geometry in such scenarios. Custom-made algorithms should find a middle way between the solution accuracy and computational cost.

5. AKNOWLEDGEMENTS

The authors are extremely thankful to the Spanish division of the GMV company to have provided a realistic

conjunction test case in GEO.

REFERENCES

Bom13. Claudio Bombardelli. Analytical formulation of impulsive collision avoidance dynamics. *Celestial Mechanics and Dynamical Astronomy*, 118:77–, 11 2013.

Can22. Alexia Cantoni. Numerically efficient methods for low-thrust collision avoidance maneuver design in geo regime. Master's thesis, School of industrial and information engineering, Department of aerospace science and technology, Politecnico di Milano, Italy, 2022.

CB94. Genevieve Campan and Pascal Brousse. Orange: Orbital analytical model for geosynchronous satellite. *Journal of The Brazilian Society of Mechanical Sciences*, 16:561–572, 01 1994.

Dea98. R Deakin. Derivatives of the earth's potentials. *Geomatics Research Australasia*, pages 31–60, 1998.

ESA22. ESA. Space debris problem, 2022.

GAL+16. Clément Gazzino, Denis Arzelier, Damiana Losa, C. Louembet, Christelle Pittet, and L. Cerri. Optimal control for minimum-fuel geostationary station keeping of satellites equipped with electric propulsion. *IFAC-PapersOnLine*, 49, 12 2016.

Gaz17. Clément Gazzino. Dynamics of a Geostationary Satellite. (Rapport LAAS n° 17432), November 2017.

GGCDL19. JL Gonzalo Gomez, C Colombo, and P Di Lizia. A semi-analytical approach to low-thrust collision avoidance manoeuvre design. In *70th International Astronautical Congress (IAC 2019)*, pages 1–9, 2019.

HAB21a. Javier Hernando-Ayuso and Claudio Bombardelli. Low-thrust collision avoidance in circular orbits. *Journal of Guidance, Control, and Dynamics*, pages 1–13, 2021.

HAB21b. Javier Hernando-Ayuso and Claudio Bombardelli. Low-thrust collision avoidance in circular orbits. *Journal of Guidance, Control, and Dynamics*, 44(5):983–995, May 2021.

LKS12. Sang-Cherl Lee, Hae-Dong Kim, and Jinyoung Suk. Collision avoidance maneuver planning using ga for leo and geo satellite maintained in keeping area. *International Journal of Aeronautical and Space Sciences*, 13:474–483, 2012.

LLD+06. Damiana Losa, Marco Lovera, Remi Drai, T. Dargent, and Joël Amalric. Electric station keeping of geostationary satellites: a differential inclusion approach. pages 7484 – 7489, 01 2006.

MCBHA21. Álvaro Martínez Chamarro, Carlos Belmonte Hernandez, and Roberto Armellin. Design of collision avoidance maneuvers using optimal control theory and convex optimization. *31st Space Flight Mechanics Meeting*, 2021.

Pal21. Maria Francesca Palermo. Numerically efficient methods for impulsive and low-thrust collision avoidance manoeuvre design. Master's thesis, School of industrial and information engineering, Department of aerospace science and technology, Politecnico di Milano, Italy, 2021.

RS18. Jason A Reiter and David B Spencer. Solutions to rapid collision-avoidance maneuvers constrained by mission performance requirements. *Journal of Spacecraft and Rockets*, 55(4):1040–1048, 2018.

Soo94. E.M. Soop. Handbook of geostationary orbits. 1994.